Implications of yield penetration on confinement requirements of r.c. wall elements

Souzana P. Tastani[*1] and Stavroula J. Pantazopoulou[2a]

[1]*Department of Civil Engineering, Democritus University of Thrace (DUTh), Vas. Sofias 12, 67100, Greece*
[2]*Department of Civil and Environmental Engineering, University of Cyprus, Nicosia 1687, Cyprus*

Abstract. Seismic-design procedures for walls require that the confinement in the critical (plastic hinge) regions should extend over a length in the compression zone of the cross section at the wall base where concrete strains in the Ultimate Limit State (ULS) exceed the limit of 0.0035. In a performance-based framework, confinement is linked to required curvature ductility so that the drift demand at the performance point of the structure for the design earthquake may be met. However, performance of flexural walls in the recent earthquakes in Chile (2010) and Christchurch (2011) indicates that the actual compression strains in the critical regions of many structural walls were higher than estimated, being responsible for several of the reported failures by toe crushing. In this study, the method of estimating the confined region and magnitude of compression strain demands in slender walls are revisited. The objective is to account for a newly identified kinematic interaction between the normal strains that arise in the compression zone, and the lumped rotations that occur at the other end of the wall base due to penetration of bar tension yielding into the supporting anchorage. Design charts estimating the amount of yield penetration in terms of the resulting lumped rotation at the wall base are used to quantify the increased demands for compression strain in the critical section. The estimated strain increase may exceed by more than 30% the base value estimated from the existing design expressions, which explains the frequently reported occurrence of toe crushing even in well confined slender walls under high drift demands. Example cases are included in the presentation to illustrate the behavioral parametric trends and implications in seismic design of walls.

Keywords: bond; anchorage; yield penetration; lumped rotation; confinement boundary element

1. Introduction

The M8.8 Richter earthquake that occurred in February of 2010 in Chile was marked by several wall failures - field observations identified several compression failures particularly in slender walls (in high-rise buildings, EC8-I 2004). This raised some anxiety in the engineering community, following the recent shift to displacement-based design of walls (in EC8-I and ACI318) according to which, confinement requirements were to be linked to the estimated compressive strain demand at the wall toe. Clearly, success of displacement-based design of walls

---

∗Corresponding author, Lecturer, E-mail: stastani@civil.duth.gr
[a]Professor, E-mail: pantaz@ucy.ac.cy, pantaz@civil.duth.gr

rides on the dependability of the compression strain estimate. But the evidence from the Chile failures suggests that strains well beyond the spalling/crushing limit of unconfined concrete developed during this M8.8 Richer earthquake.

Further evidence resulting from comparison between analytical with experimental values of compressive strain in reinforced concrete shear walls bent in flexure have shown that there is a consistent tendency for underestimation of concrete's deformations in the compression zone. For example, several experimental studies point to a higher than estimated compressive strain in the compression zone of slender walls tested under reversed cyclic loading (Aaleti 2009, Aaleti *et al.* 2013, Beyer *et al.* 2011, Birely *et al.* 2008, Birely *et al.* 2010, Dazio *et al.* 2009, Elnashai *et al.* 1990, Hiraishi 1984, Hannewald *et al.* 2012, Johnson 2010, Massone and Wallace 2004, Oesterle *et al.* 1976, Oesterle *et al.* 1979, Thomsen and Wallace 1995, 2004, Wallace *et al.* 2012). This finding is consistent with the aforementioned compression crushing failures at the base corner of structural walls (Wallace and Moehle 2012).

In this paper this phenomenon is explored from first principles. The reported compression crushing failures are interpreted in light of the kinematics of a structural wall which are effected by the pullout slip of longitudinal tension reinforcement. This source of compression strain demand has not been considered before, possibly because researchers used to account for the increased confinement in the wall toe region caused by the presence of the stiff footing. A short description of the problem and its relevant parameters is given in the remainder of this section.

Slender walls usually occur in high rise structures for which $T_1 > T_C$, where, T_1 is the fundamental period of the building and T_C is the period at the upper limit of the constant acceleration region of the total acceleration design spectrum. Therefore, EC8-I (2004) assumes that an upper limit to curvature ductility demand μ_ϕ, may be estimated from the behavior factor q through the relationship (based on the equal displacement rule)

$$\mu_\phi = 2q - 1 \quad for \quad T_1 > T_C \tag{1a}$$

Otherwise

$$\mu_\phi = 1 + 2(q-1)\frac{T_C}{T_1} \quad for \quad T_1 < T_C \tag{1b}$$

According to the EC8-I (2004), in critical regions of primary seismic elements with longitudinal reinforcement of steel class B (medium ductility) the available curvature ductility capacity μ_ϕ should be at least equal to 1.5 times the value given by the Eq. (1). The external most stressed part of the compression zone of the critical wall section is required to be confined by a mechanical reinforcement ratio, $a \cdot \omega_{wd}$ (EC8-I 2004) that exceeds the limit

$$a \cdot \omega_{wd} \geq 30\mu_\phi(\nu_d + \omega_v) \cdot \varepsilon_{sy,d} \frac{b_w}{b_o} - 0.035 \tag{2a}$$

$$\text{with } \omega_{wd} \geq \begin{array}{l} 0.08 \ for \ q = 3.5 \\ 0.12 \ for \ q = 5 \end{array} \tag{2b}$$

$$\text{and } a = \left[1 - \sum_{i=1}^{n}\frac{b_i^2}{6A_g(1-\rho_v)}\right] \cdot \left[1 - \frac{s'}{2b_o}\right]^2 \tag{2c}$$

Parameters in Eq. (2) include, the mechanical ratio of vertical web reinforcement, $\omega_v=\rho_v f_{yd,v}/f_{cd}$, and the $_d$ subscript identifies design material values (which are taken equal to the characteristic values for the seismic combination); the confinement effectiveness coefficient a, defined for the boundary element region (this is estimated in a standard way as per Eq. (2c), e.g., Priestley et al. 1996). Also, ε_{sy} is the steel yielding strain (Fig. 1(b)), v_d the normalized applied axial load ratio, b_w is the thickness of the wall section, b_o is the width of the confined core in the boundary element of a wall (Fig. 1(a)), s' is the clear spacing between successive stirrups, and b_i is the distance between parallel vertical bars in the confined boundary element region. The length of the wall end that need be confined (confined boundary element) measured from the centroid of the outside stirrup is equal to (Fig. 1(a))

$$l_c = x_u \cdot \left(1 - \frac{\varepsilon_{cu}}{\varepsilon_{cc,u}}\right) \quad ; \quad \varepsilon_{cc,u} = 0.0035 + 0.1 \cdot a \cdot \omega_{wd} \tag{3}$$

where, term ε_{cu} is the strain at compression spalling (taken for simplicity equal to 0.0035 according
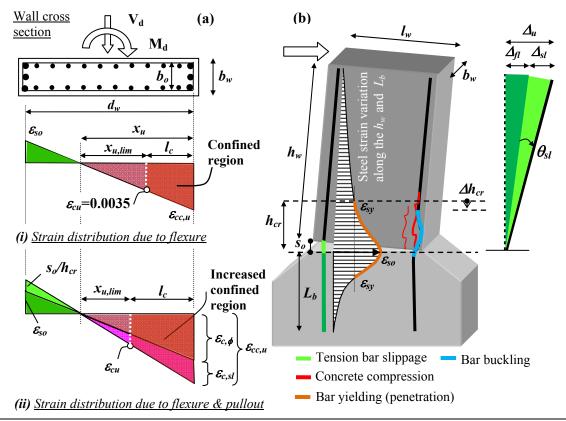

Fig. 1 Definition of terms: (a) Limits of the confined boundary element defined by considering (i) only flexural response and (ii) flexural and pullout response. (b) Cantilever model for deformation analysis of a shear wall. The hatched diagram represents a smoothened distribution of bar strains in the longitudinal tension reinforcement. The length over which strains exceed the yielding strain is length of yield penetration, occurring on both sides of the critical section

to European design practice) and $\varepsilon_{cc,u}$ is the strain capacity of confined concrete. Thus, special transverse reinforcement is required over that part of the compression zone (i.e., over a length of l_c) where the compressive strains exceed the crushing strain of unconfined concrete, ε_{cu}=0.0035 (EC8-I 2004, Fig. 1(a)).

According to Eq. (3) and Fig. 1(a-i) the check of the compressive strains along the compressive zone, x_u, is converted to a check for the depth of compression zone against a limiting value, $x_{u,lim}$, associated with attainment of the ε_{cu}=0.0035. The threshold value of $x_{u,lim}$ is defined by Eq. (4) where term θ_{pl} is the local plastic hinge rotation at the wall base, defined as Δ_u/h_w with Δ_u being the total peak displacement demand (Fig. 1(b)) for the wall structure, h_w is the wall height (measured from the critical cross-section up to the estimated point of inflection; for structures with relatively flexible diaphragms such as flat slabs, h_w may be taken equal to the wall height), and h_{cr} is the plastic hinge length (this is the length in the clear height of the wall where yield penetration may occur - and it is generally much lower than the design length of critical region which is used for detailing). For slender walls, h_{cr} is taken up to half the length of the wall cross section, l_w (Wallace and Moehle 2012). Term Δ_u is estimated from the design earthquake (from spectral displacement, S_d, as $\Delta_u=S_d\cdot C_d$ where S_d is obtained from spectral acceleration S_a, according with, $S_d=S_aT_1^2/(4\pi^2)$, and C_d is a coefficient around 1.3 required to convert spectral displacement to displacement of the structure). In design, the ultimate drift ratio demand is set equal to the local plastic hinge rotation at the wall base, θ_{pl}. The extreme fiber compressive strain $\varepsilon_{cc,u}$, at the critical cross section is obtained as

$$
\left.\begin{array}{l}
\theta_{pl} = \dfrac{\Delta_u}{h_w} = \phi_u \cdot h_{cr} \\[2mm]
\phi_u = \dfrac{\varepsilon_{cc,u}}{x_u} = \dfrac{0.0035}{x_{u,lim}} = \dfrac{\mu_\phi \cdot \varepsilon_{sy}}{d_w - x_u}
\end{array}\right\}
\quad
\begin{array}{l}
\Rightarrow \quad \varepsilon_{cc,u} = \dfrac{\theta_{pl}}{h_{cr}} \cdot x_u = 2\dfrac{\Delta_u}{h_w}\cdot\dfrac{x_u}{l_w} \\[3mm]
\Rightarrow \quad x_{u,lim} = 0.0035 \cdot \dfrac{h_{cr}}{\theta_{pl}} \approx \dfrac{l_w}{600\cdot\theta_{pl}}
\end{array}
\tag{4a}
$$

Combining Eqs. (2)-(3) regarding the strain $\varepsilon_{cc,u}$, Eq. (4a) results in

$$
\varepsilon_{cc,u} = 0.0035 + 0.1\cdot a\cdot\omega_{wd} = \dfrac{\theta_{pl}}{h_{cr}}\cdot x_u \quad \Rightarrow \quad x_u = \dfrac{h_{cr}}{\theta_{pl}}\cdot\left(0.0035 + 0.1\cdot a\cdot\omega_{wd}\right)
\tag{4b}
$$

Thus, according to Eq. (4a), when $x_u > x_{u,lim}$, confined boundary elements are required in the length $l_c=(x_u-x_{u,lim})$. In ACI318 (2011) the required confined boundary element length is determined according to the previously detailed procedure. The EC8-I (2004) requires that $l_c=x_u-x_{u,lim}\geq\max[0.15l_w, 1.5b_w]$ in order for the wall to provide the required deformation capacity. Also, Eq. (4b) relates the length of the compression zone x_u with the attained plastic hinge rotation and the confinement detailing of the critical cross section. Combining Eqs. (4a)-(4b) the following may be derived

$$
l_c = \dfrac{h_{cr}}{\theta_{pl}}\cdot 0.1\cdot a\cdot\omega_{wd} \approx \dfrac{l_w}{\theta_{pl}}\cdot 0.05\cdot a\cdot\omega_{wd} \quad \Rightarrow \quad \theta_{pl} = \dfrac{l_w}{l_c}0.05\cdot a\cdot\omega_{wd}
\tag{4c}
$$

Therefore, the rotational capacity of the wall, θ_{pl} is limited by the available amount of boundary confinement (i.e., the mechanical reinforcement ratio, $a\cdot\omega_{wd}$).

2. Kinematics of yield penetration and pullout rotation

Yield penetration is known to destroy interfacial bar - concrete bond; the length over which it occurs is marked by substantial bar strains exceeding the value of ε_{sy} (Fig. 1(b)). The effect of yield penetration above the critical section (in the plastic hinge zone) is included in the estimation of plastic rotation of the cantilever. On the other hand, the effect of yield penetration which occurs inside the pedestal is included in the estimated bar pullout slip, s, which represents the width of the crack opening at the base of the wall. Slip is estimated from the integration of bar strains over the length of anchorage. Therefore, slip is increased significantly with the occurrence of yield penetration. This affects the plastic rotation capacity of the member by increasing the contribution of bar pullout. As a result, secondary axial strains are enforced in the compression zone within the plastic hinge region of structural walls, which may be critical in the displacement-based detailing procedures that link confinement of walls to compressive strains (EC8-I 2004).

The compressive strain in the compression zone of shear walls could be affected significantly by the lumped rotation at the critical cross section near the face of the support due to pullout of the tension reinforcement from its anchorage (for definition of terms see Eq. (6b) in the relevant section). In this case damage is concentrated in a single large crack at the foundation-wall interface (Fig. 2(a)). Several studies indicate that an important part of the total drift ratio in slender walls may be owing to pullout slip at the pedestal (Wallace and Moehle 2012). Johnson (2010) and Aaleti *et al*. (2013) list explicit experimental measurements of the drift components that result
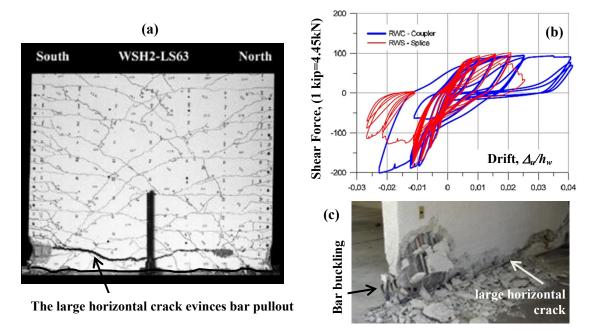

Fig. 2 (a) Shear wall failure due to concrete crushing of the cross section compression zone and development of a single wide crack at the foundation-wall interface (Dazio *et al*. 2009). (b) Increased total drift as a result of the lumped rotation due to tension reinforcement pullout from its anchorage (from the experiment by Aaleti *et al*. 2013). (c) Buckling of bars due to excessive compression strain induced from tension bar pullout from its anchorage

from strain penetration in the pedestal in slender walls. Other researchers lump a part of the rotation due to pullout slip in the flexural plastic rotation, θ_{pl}, by extending the definition of the plastic hinge length to include the front segment of yield penetration in the pedestal (see for example, Dazio *et al.* 2009); in these cases the reported pullout rotation that is estimated from strains developing in the residual anchorage length inside the pedestal may be significantly smaller.

Because the compression zone cannot penetrate into the support as would be required by the kinematics of rotation in the critical section (assuming the familiar cantilever model, Fig. 1(b)), the region of the member adjacent to the support is forced to undergo increased contraction strain in order to accommodate the effects of this rotation. The associated kinematic relationship, given by Eq. (5), has been proposed by Syntzirma *et al.* (2010) to account for this localized compression strain increase, which states that the compressive strain at the extreme fiber of the cross section, $\varepsilon_{cc,u}$, in the plastic hinge region of a flexural member is the sum of two contributions:

(i) the strain $\varepsilon_{c,\phi}$ due to sectional flexural curvature ϕ (i.e., $\phi = \varepsilon_{c,\phi}/x_u = \varepsilon_{so}/(d_w - x_u)$), where x_u is the depth of compression zone, ε_{so} is the axial strain in the tension reinforcement at the critical section and d_w is the effective depth of the wall cross-section -taken here as $0.8 l_w$ where l_w is the wall section length), and

(ii) the strain $\varepsilon_{c,sl}$ (see Fig. 1(a-ii)); this term may be calculated by considering the additional shortening of the compression fibers, Δh_{cr}, which occurs within the plastic hinge length h_{cr} and on the compression side of the member, in order for the member to accommodate the rotation, θ_{sl}, at the critical section due to pullout s_o of tension reinforcement (Fig. 1(b)). The shortening Δh_{cr} is distributed over h_{cr} leading to the estimation of an equivalent average compression axial strain component, $\varepsilon_{c,sl}$

$$\varepsilon_{c,\phi} = \varepsilon_{so} \cdot \frac{x_u}{d_w - x_u}; \qquad \Delta h_{cr} = s_o \cdot \frac{x_u}{d_w - x_u}; \qquad \varepsilon_{c,sl} = \frac{\Delta h_{cr}}{h_{cr}} = \frac{s_o}{h_{cr}} \cdot \frac{x_u}{d_w - x_u} \tag{5a}$$

therefore

$$\varepsilon_{cc,u} = \varepsilon_{c,\phi} + \varepsilon_{c,sl} = \varepsilon_{so} \cdot \frac{x_u}{d_w - x_u} + \frac{s_o}{h_{cr}} \cdot \frac{x_u}{d_w - x_u} = \left(\varepsilon_{so} + \frac{s_o}{h_{cr}} \right) \cdot \frac{x_u}{d_w - x_u} \tag{5b}$$

The length of the plastic hinge region, h_{cr}, (where strains are greater than ε_{sy}) is taken up to a maximum of $0.5 l_w$. In design, a much higher value is assumed for h_{cr}, in order to enforce greater amounts of detailing in the lower storey of wall-buildings (EC8-I 2004). Through detailing the objective is to prevent the compression zone from bulging out as shown in Fig. 2(c). A schematic representation of Eq. (5) which accounts for flexural and slip contributions on sectional curvature is shown in Fig. 1(a-ii); for comparison, the conventional distribution of sectional deformations under the loading combination N+M are also depicted in Fig. 1(a-i).

For usual values of the axial load ratio, v_d, (i.e., for $v_d < 0.45 = v_{d,bal}$), the depth of compression zone x_u is usually less than half the cross section height, $0.5 l_w$. This may be said in light of the fact that the compression zone depth at balanced conditions with $v_{d,bal} = 0.45$ is, $x_u = 0.47 l_w$ ($= \varepsilon_{cu}/(\varepsilon_{cu} + \varepsilon_{sy}) \cdot d_w = 0.0035/(0.0035 + 0.0025) \cdot 0.8 l_w$, where tension steel is at yielding (i.e., $\varepsilon_s = 0.0025$) and the extreme compression strain of concrete reaches its ultimate unconfined value of 0.0035).

Eq. (5) highlights a newly identified interaction between flexural action and pullout behavior of the reinforcement: evidently, bar slip affects sectional equilibrium through the effect it has on strain $\varepsilon_{cc,u}$. Given the sectional geometry and the materials stress-strain laws, the resulting moment

- curvature (M-ϕ) relationship at the critical cross section is no longer unique for a given axial load value, but it depends on the details and the state of stress in the reinforcement anchorage. Objective of the paper is to identify the practical implications of yield penetration on rotation capacity (i.e., Δ_u) and the associated confinement requirements (i.e., $x_{u,lim}$) of shear walls.

3. Effects on compression strain demand

To identify the implications that slip of tension reinforcement has on the concrete compressive strain a practical example is considered: the wall cross section has a width of b_w=200 mm and height l_w=1000 mm (d_w=0.8l_w=800 mm) whereas the assumed plastic hinge length is h_{cr}=0.5l_w; for a compression zone depth x_u=0.25l_w=250 mm and axial tensile strain in the boundary longitudinal reinforcement, ε_{so}=0.006 (beyond yielding) the state of the cross section at the wall base is evaluated. The corresponding value of $\varepsilon_{cc,u}$ is 0.0027 if slip is ignored (i.e., s_o=0 in Eq. (5)), but for as small a slip value as s_o=2 mm the corresponding concrete strain $\varepsilon_{cc,u}$ is increased to 0.0045, hence the extreme fibers of the compression zone are at a state of crushing. Thus, the increase of compressive strain $\varepsilon_{cc,u}$ in the plastic hinge zone due to anchorage pullout drives the concrete to enter faster in its stress -strain softening branch. If confinement is absent then the longitudinal reinforcement on the compression side is susceptible to imminent bar buckling (see Fig. 2(c)) which is usually accompanied with bar fracture on the tension side (Jiang *et al*. 2013).

The slippage of the tension reinforcement is also accounted for in the value of total peak displacement Δ_u by considering that the latter is the sum of the flexural and the pullout contributions, Δ_{fl} and Δ_{sl}, as depicted in Fig. 1(b). Thus, the increase of peak displacement due to slippage results in the reduction of the estimated $x_{u,lim}$ as per Eq. (4a) and to a commensurate increase of the required confined depth of the shear wall as illustrated in Fig. 1(a-ii).

Equation (5) underlines the importance of dependably estimating bar slip, s_o, as a prerequisite to accurately evaluating the state of stress in the critical cross section of shear walls adjacent to monolithic connections. When the bar is strained beyond yielding, a large fraction of the slip measured in tests is owing to inelasticity spreading over the bar anchorage, known as yield penetration.

Calculation of slip in yielding anchorages is essential for accurate interpretation of the reported failures described in the preceding. These implications concern a number of different aspects:

• The excessive amount of reinforcement slip from the yielded anchorage increases the flexibility of the member connection to its support, where a fraction of the rotation is owing to reinforcement pullout from the anchorage rather than from flexural curvature over the member length.

• The kinematics of rotation due to bar pullout causes increased strains in the compression zone of the member, particularly within the length of the plastic hinge zone h_{cr} adjacent to the support (see Fig. 1(b)). Performance-based detailing of certain structural members is controlled by the amount of concrete compression strains (e.g., structural walls, EC8-I and ACI318 Chapter 21). In these cases, the effects of yield penetration may counteract the design objective due to the higher attained compressive strain magnitudes as compared with the assumed values.

• It is shown that yield penetration may limit the strain development capacity of longitudinal reinforcement, an issue that is particularly important in existing construction where either the available anchorage is limited, or, the structural member has undergone yielding during previous
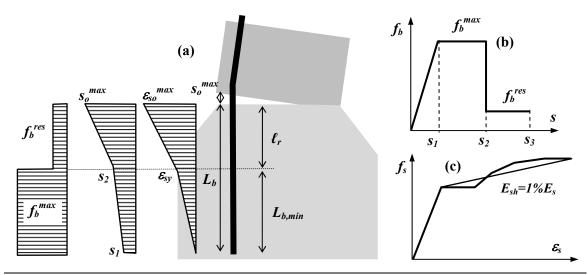
Fig. 3 (a) Attenuations of inelastic bar strain capacity and the associated bond stress and slip along the anchorage. (b) Simplified elasto-perfectly plastic with a post-peak residual plateau bond-slip law. (c) Idealized bilinear stress strain relationship of longitudinal reinforcement

seismic events thereby exhausting part of the dependable strain capacity of the anchorage of primary reinforcement. To address these issues the equations for bond of yielding rebars (Tastani and Pantazopoulou 2013a, 2013b) are applied to explore the bar strain development capacity over yielded anchorages.

4. Bar anchorage strain development capacity

The solution developed in this section evaluates the strain development capacity of a bar with an idealized bilinear stress-strain curve having a post-yielding hardening slope, E_{sh} (no plateau), anchored in concrete over a length L_b (Fig. 3(a)); the assumed bond-slip curve has the characteristics depicted in Fig. 3(b). The maximum slip, s_o^{max}, that may be developed by the straight part of a bar anchorage (i.e., if a hook detailing is present) at the critical cross section of the shear wall is given by Eq. (6a). It consists of three contributions (Tastani and Pantazopoulou 2013a, 2013b), namely:

   • the slip of the anchorage end point at imminent anchorage failure, which is set equal to the slip at the end of the ascending branch of the local bond-slip law, s_1 (Figs. 3(a)-(b)),

   • the slip owing to integration of the linearly varying bar strains - from zero at the anchorage end point, to the point where yield strain ε_{sy} is developed along a minimum required bonded length, defined as: $L_{b,min} = D_b/4(f_{sy}/f_b^{max})$ as $1/2\varepsilon_{sy} \cdot L_{b,min}$ (thus $s_2 = s_1 + 1/2\varepsilon_{sy} \cdot L_{b,min}$) and,

   • the slip due to yield penetration over the *maximum sustainable debonded length (MSDL)*, which is estimated from: $\ell_r = (L_b - L_{b,min})$ as $1/2(\varepsilon_{sy} + \varepsilon_{so}^{max})\ell_r$.

$$s_o^{max} = s_1 + \frac{1}{2}L_b\varepsilon_{sy} + \frac{1}{2}\left(L_b - L_{b,min}\right) \cdot \varepsilon_{so}^{max} \tag{6a}$$

Therefore, the definition of an MSDL is based on the postulate that prior to complete anchorage failure, the bar has become gradually debonded from concrete over the length ℓ_r due to yielding, so that the residual bonded length is just adequate to develop the bar force as required by equilibrium, and that any further increase in the bar strain at the critical section leads to pullout failure. At that reference point of imminent anchorage failure, the lumped rotation at the base of the wall may be estimated from (definition of θ_{sl} is depicted in the right-hand side of Fig. 1(b))

$$\theta_{sl} = \frac{\Delta_{sl}}{h_w} = \frac{s_o^{max}}{d_w - x_u} \tag{6b}$$

The associated tensile strain capacity of the reinforcement, i.e., the maximum strain that may be developed by the anchorage, ε_{so}^{max}, and the corresponding bar strain ductility, $\mu_{\varepsilon s}$, are given by Eq. (7)

$$\varepsilon_{so}^{max} = \varepsilon_{sy} + 4 \cdot \left(L_b - L_{b,min}\right) \frac{f_b^{res}}{D_b E_{sh}} \quad ; \quad \mu_{\varepsilon s} = \frac{\varepsilon_{so}^{max}}{\varepsilon_{sy}} = 1 + 4 \cdot \frac{L_b - L_{b,min}}{D_b} \cdot \frac{f_b^{res}}{E_{sh} \cdot \varepsilon_{sy}} \tag{7}$$

Term f_b^{res} is the residual bond resistance (see the degraded end of the bond-slip law in Fig. 3(b), and D_b is the bar diameter.

Eq. (7) is investigated below with regards to the important parameters through a sensitivity study based on the analytical model presented in Tastani and Pantazopoulou (2013a, 2013b). Fig. 4(a) plots the estimated strain ductility capacity $\mu_{\varepsilon s} = \varepsilon_{so}^{max}/\varepsilon_{sy}$ of a straight anchored bar, which can be supported by the normalized anchorage length L_b/D_b (a parameter of study), for steel class S500-C (where the yielding strength is f_{sy}=500MPa, f_{su}=575MPa, ε_{su}>7.5%). Five different concrete types are considered, (with f_c'=30MPa, 25MPa, 20MPa, 16MPa and 12MPa), two bond conditions (the characteristic bond strength, f_b^{max} was taken equal to $2.5\sqrt{f_c'}$ and $1.25\sqrt{f_c'}$ for good and all other bond conditions respectively, values taken from Table 1 in accordance with *fib* MC2010) and two values for the hardening modulus of steel reinforcement (1% and 5% of E_s=200GPa). The residual bond strength f_b^{res} (attained after bar yielding, thus ε_{so}^{max}>ε_{sy}) was estimated according with the local bond model prescribed by the fib Model Code (2010) (see Tastani and Pantazopoulou 2013a). In Fig. 4(a) the lower the concrete quality, the thinner the line of the corresponding curve. Note that the method to develop such diagrams has been presented elsewhere (Tastani and Pantazopoulou 2013a). (In case there is a hooked anchorage, the straight length used in the calculations or in the charts is extended by ΔL_b=12.5D_b - note that according with the Model Code (2010) the strength of an anchored bar is increased by $50A_b f_{bmax}$ by the presence of a hook, i.e., the value of ΔL_b).

Similar diagrams to those of Fig. 4(a) are produced by using the design bond strength f_{bd} (nominal values are included in the fourth line of Table 1 and are calculated as per the *fib* MC2010

Table 1 Bond strength values for anchorage pullout failure and $\varepsilon_{so} \leq \varepsilon_{sy}$ (*fib* MC2010)

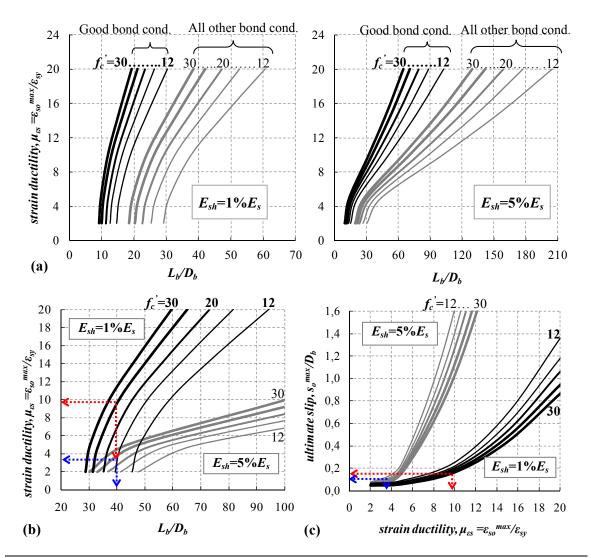| f_c' (MPa)	12	16	20	25	30
Good bond conditions: f_b^{max}=$2.5\sqrt{f_c'}$ (MPa)	8.7	10	11.2	12.5	13.7
All other bond conditions: f_b^{max}=$1.25\sqrt{f_c'}$ (MPa)	4.3	5	5.6	6.3	6.8
For *S500* & $D_b \leq 20$ mm: f_{bd}=$2 \cdot f_{bo}$= =$2 \cdot n_1 n_2 n_3 n_4 (f_c'/20)^{0.5}$	2.8	3.2	3.6	4.0	4.4

Fig. 4 (a) Anchorage strain ductility capacity versus the required anchorage length for steel category **S500**, two values for hardening modulus (E_{sh}=1% and 5%E_s), five concrete strengths (f_c'=12, 16, 20, 25, 30 MPa) and two bond conditions (see Table 1). Using design bond strength f_{bd} values (4th line of Table 1): (b) diagrams μ_{es} - L_b/D_b and (c) charts of the ultimate slip as a function of strain ductility capacity

through the expression f_{bd}=2·f_{bo}=2·$n_1 n_2 n_3 n_4(f_c'/20)^{0.5}$) rather than the value of characteristic bond strength f_b^{max} (Fig. 4(b)). Comparing the corresponding curves of Figs. 4(a)-(b) while keeping all other variables the same, i.e., E_{sh} and f_c', it becomes clear that **<u>in design</u>** (Fig. 4(b)), conservatively, the required anchorage length is longer than that calculated by using the characteristic bond strength (Fig. 4(a)) for the same target strain ductility.

To illustrate the use of Fig. 4 and also the implications of Eq. (7) on **<u>design</u>** issues let us consider a bar at the wall base with yielding stress f_{sy}=500MPa and a hardening modulus E_{sh}=5%E_s, of diameter D_b=20 mm, with design bond strength f_{bd}=4 MPa (f_c'=25 MPa, Table 1) and

s_1=0.2 mm anchored over a length L_b=800 mm (=40D_b>$L_{b,min}$=625 mm). In Fig. 4(b) the grey curve denoted by f_c'=25 MPa - E_{sh}=5%E_s and the chosen anchorage length of L_b/D_b=40 result in a strain ductility capacity of the anchorage equal to $\mu_{\varepsilon s}=\varepsilon_{so}^{max}/\varepsilon_{sy}$=3.5 (see the blue dashed line in Fig. 4(b)) and thus, the maximum strain development capacity of the reinforcement is limited to: $\varepsilon_{so}^{max}\approx$0.009, which is lower than the design ultimate strain of the reinforcement (ε_{ud}=0.02) and far less than the nominal rupture strain of the material (ε_{uk}=0.075 for class C, EC2 2004). The associated slip calculated through Eq. (6) is $s_o^{max}\approx$2 mm (or 0.1D_b - see the blue dashed line in Fig. 4(c)) whereas the lumped drift is in the order of 0.36% (d_w=800 mm, and x_u=250 mm).

Eq. (5) is used twice with the cross section data of the previous example: once without and once with due consideration of the slip magnitude. These two alternatives result in a maximum confined strain demand of $\varepsilon_{cc,u}(s=0)$=0.004 and $\varepsilon_{cc,u}(s=s_o^{max})$=0.005 respectively - that is an increase by 20% in the value of peak compressive strain. For the same anchorage details, but using steel with milder strain hardening (thus E_{sh}=1%E_s, see the black curves in Fig. 4(b)) the corresponding steel strain ductility magnitudes are $\mu_{\varepsilon s}=\varepsilon_{so}^{max}/\varepsilon_{sy}$=9.5 (see the red dashed line), and thus, the strain development capacity of the reinforcement is now, ε_{so}^{max}=0.024, with $s_o^{max}\approx$3.3 mm (or 0.16D_b - see the red dashed line in Fig. 4(c)) and the corresponding confined concrete strain demands equal to $\varepsilon_{cc,u}(s=0)$=0.011, $\varepsilon_{cc,u}(s=s_o^{max})$=0.013. This highlights the significance that steel properties may have on the available deformation capacity of the anchorage. (Note that one could approximate the results of the preceding analysis without the charts of Fig. 4, by only considering values for f_b^{max}, f_b^{res}, s_1 and E_{sh} in Eqs. (6)-(7).)

The result of the first example, where E_{sh}=5%E_s, is interpreted as follows: whereas the anchorage length is sufficient for the bar to develop its yielding strength however it imposes:

• limitations regarding the available bar strain development capacity and the flexural ductility of the structural element, and

• this finding has implications on the hierarchy of failure modes of the wall cross section by seriously increasing the imposed compressive strain demands in the confined region.

5. Ductile rotation capacity associated with the anchorage deformation capacity

In design, the ultimate drift ratio demand is set equal to the local plastic hinge rotation at the wall base, θ_{pl}. Thus, it may be shown from the kinematics of the deformed member and the concrete mechanics that the term θ_{pl} comprises flexural and pullout (slip) components. Thus, $\Delta_u=\Delta_{fl}+\Delta_{sl}$ in Fig. 1(b) where, according with Eq. (6b)

$$\theta_{pl} = \frac{\Delta_u}{h_w} = \frac{\Delta_{fl}}{h_w} + \frac{\Delta_{sl}}{h_w} = \phi_u \cdot h_{cr} + \frac{s_o^{max}}{d_w - x_u} \tag{8a}$$

The cross sectional curvature, ϕ_u, is analyzed considering the anchorage tensile strain capacity of the reinforcement ε_{so}^{max} (which is a unique magnitude), leading to Eq. (8b). But if ϕ_u is obtained by considering the increased concrete compressive strain through Eq. (5) then the ultimate drift is doubly affected by the bar slippage, as shown by Eq. (8c). Note that Eqs. (5) are applicable under the requirement that the anchorage is able to develop its strain capacity ε_{so}^{max} prior to the occurrence of other, competing modes of failure (e.g., bar buckling, shear failure, limiting flexural failure).

$$\theta_{pl}(\varepsilon_{so}) = \frac{\varepsilon_{so}^{max}}{d_w - x_u} h_{cr} + \frac{s_o^{max}}{d_w - x_u} \tag{8b}$$

$$\theta_{pl}(\varepsilon_{cc,u}) = \frac{\varepsilon_{cc,u}}{x_u} h_{cr} + \frac{s_o^{max}}{d_w - x_u} \quad \overset{Eq.(5)}{\Rightarrow} \quad \theta_{pl}(\varepsilon_{cc,u}) = \frac{\varepsilon_{so}^{max}}{d_w - x_u} h_{cr} + 2\frac{s_o^{max}}{d_w - x_u} \tag{8c}$$

To illustrate the impact of bond response (through the strain capacity ε_{so}^{max} and the associated slip s_o^{max} originating at the critical cross section where the wall is connected with the pedestal) on the attained ultimate drift ratio defined by Eq. (8c), the following parametric study is presented through the diagrams of Fig. 5. For two common wall cross section lengths (i.e., l_w=1000 and 3000 mm) five levels of compression zone depths were studied. Thus, x_u=0.1, 0.2, 0.3, 0.4 and 0.5 of l_w where the thinner the curve the lower the x_u value in Fig. 5. The plastic hinge length was taken equal to h_{cr}=0.5l_w; this is deemed a conservative assumption. Tests point to concentration of damage over a wall height that is in the same range as the depth of compression zone. Thus, the effect studied would be even stronger if the strain amplification resulting from flexure-slip interaction would be taken to occur over an even shorter plastic hinge length. This point needs to be further studied through correlation with experimental data, with particular reference to the penetration of yielding into the region above the base; however the exploration of what actually defines the h_{cr} is beyond the scope of this model in its present form.

Material properties were taken as: f_c'=25 MPa and E_{sh}=1%E_s, with a nominal design bond strength value f_{bd}=4 MPa (as listed in the 4th line of Table 1 and in Fig. 4(b)). The produced diagrams relate the ultimate drift ratio with the strain ductility capacity of the anchorage and the mechanical confinement reinforcement ratio of the section, $a \cdot \omega_{wd}$. The following points are deduced:

• For a constant depth of compression zone after reinforcement yielding (e.g., here, x_u=0.4l_w) increasing the strain ductility capacity of the anchorage (for example by using a longer anchorage length) results in higher available relative drift ratio. This is secured by increasing the required confinement level (from $a \cdot \omega_{wd}$=0.3 to 0.4, see the pink dashed lines in Fig. 5(a)).

• For the same strain ductility capacity of the anchorage (e.g., here, $\mu_{\varepsilon s}$=8, which is independent of the wall geometry, and it only depends on the anchorage detailing, i.e., for constant embedded length and good bond conditions), increasing the compression zone depth x_u from 0.1 to 0.4l_w results in a higher demand for confinement reinforcement which will also be essential in order to improve the ultimate drift capacity of the wall (see the red dashed lines in Fig. 5(a)). Thus, the improvement of wall's ductility when compression depth is high (as would occur in the presence of a high axial load ratio) is secured by only providing higher confinement ratios.

• Comparing the diagrams of Figs. 5 (a)-(b) in order to establish the effect of cross section height l_w, for the same ultimate drift ratio (for example, at 2% drift, marked by the blue dot in Fig. 5) and a strain ductility capacity of the anchorage ($\mu_{\varepsilon s}$=7) it is evident that the shorter element, for a compression zone depth of x_u=0.2l_w, would require as confinement a transverse reinforcement ratio $a \cdot \omega_{wd}$=0.1. To accomplish these requirements with the longer wall element, the compression zone would have to extend over a higher fraction of the available wall length, i.e., x_u=0.3l_w (see the blue dots in Fig. 5).

Design procedure: In designing a common structural wall of orthogonal cross section, when applying ordinary code values for deformation demands (i.e., plastic drift θ_{pl} of around 2% and available strain ductility capacity $\mu_{\varepsilon s}=\varepsilon_{so}^{max}/\varepsilon_{sy}$ of the anchorage less than 10, which is ensured by
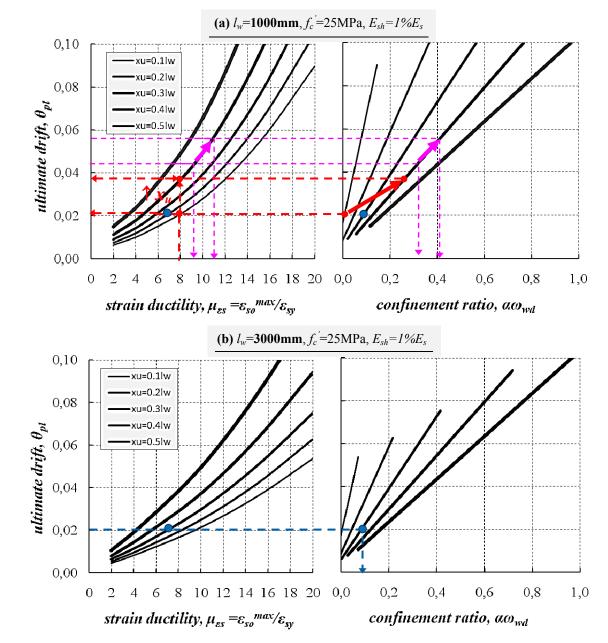
Fig. 5 Design charts that correlate the ultimate drift of a wall with the strain ductility capacity of the anchorage and the confinement reinforcement ratio for wall section heights (a) l_w=1000 mm and (b) l_w=3000 mm. (Note that the anchorage properties were taken from Fig. 4(b) for steel S500 with E_{sh}=1%E_s and concrete strength f_c'=25MPa.) Note: The lower allowable limit of confinement (EC8-I 2004) is 0.08 (for q=3.5) assuming perfect effectiveness (i.e., a=1, in Eq. (2)).

providing anchorage lengths in the order of 35 to 45D_b for common concrete qualities, i.e., 30-20 MPa), the required confinement ratios $a \cdot \omega_{wd}$ vary from very low values to 0.17 (Fig. 5) as a

function of the depth of compression zone, subject to the requirements of Eq. (2); the lower limit correspond to as small depths as $0.1l_w$ whereas the upper limit to a wider depth of $0.5l_w$. The magnitude of x_u could be found by implementing Eq. (8) for an assumed plastic hinge length h_{cr} up to $0.5l_w$ (s_o^{max} is calculated through Eq. (6a) or through Fig. 4(c)).

6. Practical implications of yield penetration – an example of a slender shear wall

A seven-storey wall structure or a total wall height of H=21 m is considered, where the expected distance to the point of moment reversal is h_w=2/3H=14 m from the base (Fig. 6a). The wall length is, l_w=3 m, and wall thickness is b_w=300 mm (thus b_o=250 mm). The axial load ratio is v=0.1. Material properties for concrete and steel are, f_c'=25 MPa, f_{sy}=500 MPa (class C[1] steel), respectively, with ε_{sy}=0.0025, E_{sh}=1%E_s (the stress-strain diagram is bi-linearized from yield to ultimate for convenience- see Fig. 3c). The wall is reinforced in the end zones with longitudinal bars having bars of diameter D_b=16 mm provided with sufficient straight anchorage inside the footing (L_b/D_b=50). For Type I elastic response spectrum (where a_g=0.36 g, with g=9.81 m/sec^2), for ground type B (thus S=1.2, T_B=0.15 sec, T_C=0.5 sec and T_D=2 sec), the period of an equivalent linear single-degree-of-freedom system is T_1=0.05·$H^{3/4}$=0.49 sec. In this case by setting the design behavior factor q equal to 3.5, it follows from Eq. (1b) that the required curvature ductility at the critical section is μ_ϕ=1+2(q-1)T_C/T_1=6.1. If the reinforcement ratio of vertical web bars in the wall is ρ_v=0.002 (resulting in a mechanical reinforcement ratio of ω_v=0.04) the lower required value of the mechanical confining reinforcement ratio, $a \cdot \omega_{wd}$, is equal to 0.0406 (by implementing Eq. (2)). In this case the strain of the extreme confined concrete fiber is $\varepsilon_{cc,u}$=0.00768 (by implementing Eq. (3)). The resulting elastic spectral acceleration demand is S_a=$a_g \cdot S \cdot 2.5$=0.36 g·1.2·2.5 thus S_a=1.08 g and the corresponding elastic displacement of the SDOF oscillator is S_d=$S_a \cdot T^2/(4\pi^2)$=0.065 m; thus the top elastic displacement of the wall, is estimated as $\Delta_{el} \approx 1.3 \cdot S_d$=0.084 m (Fig. 6a). Because $T_1<T_C$, based on EC8-I it is μ_Δ=1+(q-1)T_C/T_1=3.55 for q=3.5, thus the resultant top plastic displacement of the wall is Δ_u=$\Delta_{el} \cdot \mu_\Delta / \sqrt{(2\mu_\Delta-1)}$=0.12 m and the plastic rotation is θ_{pl}=Δ_u/H=0.12 m/21 m=0.57% (in the range of the minimum value θ_{pl}^{min}=0.7% defined by ACI 318, Chapter 21). Considering as plastic hinge length h_{cr}=0.3l_w=900 mm, implementation of Eq. (4) results in x_u=1202 mm and $x_{u,lim}$=548 mm, thus the boundary element length in each side of the section wall is l_c=x_u-$x_{u,lim} \cong$654 mm (greater than the code limit of max[0.15l_w,1.5b_w]=450 mm). The associated tensile strain demand of the longitudinal bars for $\varepsilon_{cc,u}$=0.00768 is ε_{so}=$\varepsilon_{cc,u}(d_w-x_u)/x_u$=0.00765 (here it has been assumed that the effective depth of the wall cross section is: d_w=0.8l_w).

The implications of yield penetration on the above analysis are now examined by using the charts of Fig. 6(b). Considering the anchorage geometry and the given values for the material strengths, for L_b/D_b=50 the strain ductility capacity of the anchorage is $\mu_{\varepsilon s}$=$\varepsilon_{so}^{max}/\varepsilon_{sy}$=14 thus ε_{so}^{max}

---

[1]According with EC8-I (2004) Class C steel reinforcement (recommended for seismic applications) has the following characteristics: $f_{su} \geq 1.15 f_{sy}$, $\varepsilon_{su} \geq 7.5\%$, leading to E_{sh}=0.6%E_s, which is very close to the assumed value of E_{sh}=1%E_s. Considering a less ductile class of steel (e.g., class B) would lead to higher requirements for transverse confinement according with Eq. (2), however, based on Fig. 6, the strain development capacity of the reinforcement, which depends on the anchorage (i.e., the circumstances of the reinforcement outside the member, inside the footing and when considering the implications from yield penetration) eventually will limit the performance of the wall.
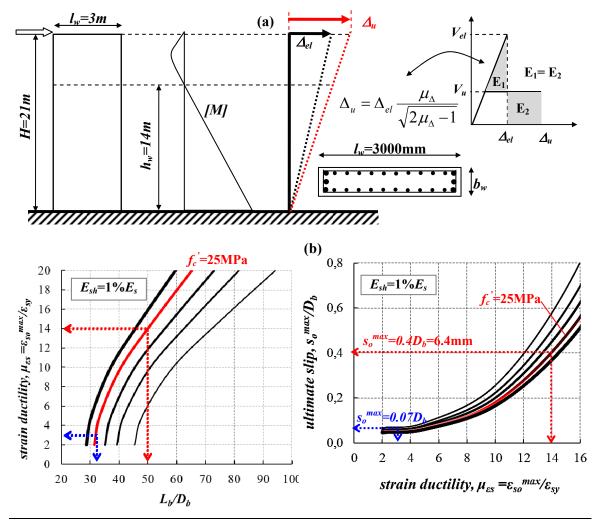
Fig. 6 (a) Geometry of the example wall and (b) the use of the anchorage detailing charts for the definition of its strain capacity and the associated slip at the critical cross section of the wall

=0.035 and s_o^{max}/D_b=0.4 thus s_o^{max}=6.4 mm. However, to account for the tensile strain demand of ε_{so}=0.00765, which corresponds to the compression strain $\varepsilon_{cc,u}$=0.00768 (in this case $\mu_{\varepsilon s}=\varepsilon_{so}/\varepsilon_{sy}$=3.06), the effective anchorage is treated as being shorter (L_b/D_b=32, blue dashed line in the left diagram of Fig. 6(b)); in this case the attained slip is defined as $s_o^{max}\approx0.07D_b$=1.1 mm. Based on the proposed model this amount of slip of the tension reinforcement imposes extra compression strain in the compressed zone of the section; implementing Eq. (5) the total compression strain is $\varepsilon_{cc,u}$=0.0089 whereas the initial plastic rotation θ_{pl}=0.57% is increased through Eq. (8a) to the value of 0.69% (the use of Eq. (8b) results in θ_{pl}=0.76%). For θ_{pl}=0.69% it is $x_{u,lim}$=454 mm (it was 548 mm), x_u=1159 mm (it was 1202 mm) whereas the boundary element length in each side of the section wall is increased from 654 mm to $l_c=x_u-x_{u,lim}\approx705$ mm. Thus, the increased compression strain as a consequence of the estimated slip (integration of tensile strain
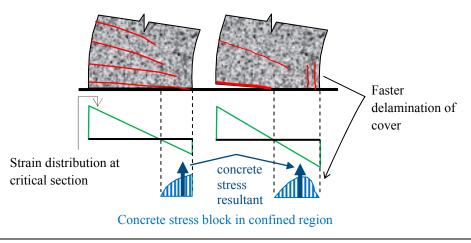
Fig. 7. The compliance in the critical wall section of high localized inelasticity in the tension reinforcement results in increased compression strains and modification of the concrete stresses due to cover delamination

along the anchorage) results in a new strain distribution along the critical cross section which now extends the already defined (by the code provisions) confined boundary element length by 50 mm. Consequently, it may be said that the compliance in the critical section with high localized inelasticity in the tension reinforcement results in increased concrete strains in the compression side that may lead to earlier onset of cover spalling. Furthermore, the increased compression strains alter the state determination on the critical wall cross section (see the difference in the concrete stress blocks in Fig. 7), since the internal stresses in the concrete are affected.

The compression strain increase by 16% as a result of yield penetration of tension reinforcement into the front part of its anchorage (which also increases the plastic rotation by 21% -from 0.57% to 0.69%) underscores the importance of confinement in order to avoid web toe crushing - a phenomenon often cited in post-earthquake reconnaissance reports - as well as in wall experimental studies. Clearly, accounting for the anchorage behavior in terms of attained slip at post-yield tensile strain demand, the boundary element geometry and confinement requirements are re-defined in order to provide the necessary resistance both to the lumped rotation due to pullout and to the increased compression strain of the wall cross section.

A notable point that is also relevant is the observation that the design code with the performance based requirement for boundary element definition focuses on the strain magnitudes inside the confined part of the compression zone, thereby accepting cover spalling at the toe, for the performance level considered. Yet, cover spalling removes a sizeable part of the lateral resistance of longitudinal reinforcement in the compression zone, against buckling. But recent studies suggest that additional measures such as externally bonded FRP layers wrapped locally around the toe and anchored over the length of the boundary element will preclude cover delamination thereby eliminating even this occurrence of damage (Fardis *et al.* 2013).

7. Conclusions

Pullout rotation resulting from yield penetration at the base of walls undergoing large lateral

drifts effectively increases the magnitude of compression strain demands and the amount and extent over the wall length where boundary element confinement should be provided, the most critical being the ends where cover spalling is unavoidable in the absence of pertinent external confinement. A mechanistic model was developed in this paper in order to evaluate this effect. The model was used to illustrate a number of consequences in practical design as follows:

(i) Current methods for analysis of wall cross sections do not consider the kinematic interaction between flexure and reinforcement pullout slip. Thus, in designing for reinforcement anchorage, the emphasis is on the ability of the anchorage to develop the yield stress of the reinforcement.

(ii) The occurrence of bar strains that exceed the yielding limit at the critical section of the walls necessarily implies that a certain amount of yield penetration occurs over the anchorage. Because bond is eliminated over the yielded portion of the bar, yield penetration effectively limits the available development length, and the tensile strain development capacity of an anchorage.

(iii) In a displacement-based design framework, the strain demand imposed on the anchorage of tension reinforcement is determined from the target drift at the performance point. It is therefore essential to compare this strain demand with the available strain development capacity of the anchorage.

(iv) Increasing the strain ductility capacity of the anchorage (for example by using a longer anchorage length) results in a higher relative drift ratio capacity. However, due to the kinematic interaction, this requires much higher compressive strains and a longer boundary element length in the compression zone of the wall. This may be secured by increasing the confinement level of the boundary elements.

(v) For a given strain development capacity of the anchorage of wall tension reinforcement, increasing the compression depth x_u results in a higher demand for confinement reinforcement. Increased confinement also benefits the drift capacity of the wall.

(vi) Regarding the effect of cross section height l_w, for the same ultimate drift demand and strain ductility capacity of the anchorage, keeping identical the transverse reinforcement ratio, the more slender wall would require a shorter fraction of its length as compression zone depth.

(vii) The topic of higher than expected strain in the compression zone has not been considered before, possibly because researchers used to postulate a confining influence by the adjacent stiff pedestal/footing. Future research should consider this effect in determining the required lengths of confined boundary elements (but also innovative confining schemes) so as to prevent the cover spalling that will precede realization of the high compressive strains which are estimated to occur within the confined wall boundary element.

Further developments in practical seismic design of walls are still needed to preclude the type of wall damage seen in the recent devastating earthquakes of Chile (2010) and New Zealand (2011). Many other phenomena may be also responsible for the observed crushing failures in these events, (Dazio *et al*. 2009, Wallace and Moehle 2012, Wallace *et al*. 2012) such as slenderness of the wall when subjected to structural displacements orthogonal to the wall's plane of action that may mobilize second order effects.

Open issues include: (i) The analytical definition of the critical plastic hinge length h_{cr} with particular reference to the penetration of yielding into the region above the base and its verification with experimental data. (ii) The importance of flexure-slip interaction particularly in shorter anchorages/lap-splices or in less favorable bond conditions (such as would prevail in field examples of older structures) where yield-penetration results in significant pullout slip values. (iii) The effect studied is also expected to cause excessive compression strains in the longitudinal reinforcement in the compression zone of the wall base cross section, leading to the symmetric

buckling patterns that were observed in field reconnaissance reports. Thus prioritizing the involved competing failure modes (bar buckling higher than concrete crushing) modifications would be necessary regarding the lateral support conditions of the compression reinforcement (with reference to the stirrup spacing, s/D_b).s

References

Aaleti, S. (2009), "Behavior of rectangular concrete walls subjected to simulated seismic loading", Ph.D. thesis, Department of Civil, Construction and Environmental Engineering, Iowa State University, Ames, IA, USA.

Aaleti, S., Brueggen, B., Johnson, B., French, C. and Sritharan, S. (2013), "Cyclic response of reinforced concrete walls with different anchorage details: experimental investigation", *J. Struct. Eng.*, ASCE, **139**(7), 1181-1191.

ACI 318 (2011), *Building Code Requirements for Structural Concrete (ACI 318M-11) and Commentary*, American Concrete Institute, Farmington Hills, U.S.A. ISBN 978-0-87031-745-3.

Beyer, K., Dazio, A. and Priestley, N.M.J. (2011), "Shear deformations of slender reinforced concrete walls under seismic loading", *ACI Struct. J.*, **108**(2), 167-177.

Birely, A., Lehman, D., Lowes, L., Kuchma, D., Hart, C. and Marley, K. (2010), "Investigation of the seismic response of planar concrete walls", 9th U.S. National Conference and 10th Canadian Conference on Earthquake Engineering, Ontario, Canada.

Birely, A., Lehman, D., Lowes, L., Kuchma, .D, Hart, C. and Marley, K. (2008), "Investigation of the seismic behavior and analysis of reinforced concrete structural walls", *14th World Conference on Earthquake Engineering*, Beijing, China.

Dazio, A., Beyer, K. and Bachmann, H. (2009), "Quasi-static cyclic tests and plastic hinge analysis of RC structural walls", *Eng. Struct.*, **31**(7), 1556-1571.

EC2 (2004), *BS EN 1992-1-1: Design of concrete structures-General rules and rules for buildings*, European Committee for Standardization (CEN), Brussels.

EC8-I (2004), *Design of structures for earthquake resistance - Part 1: General rules seismic actions and rules for buildings*, European Committee for Standardization (CEN), Brussels.

Elnashai, A., Pilakoutas, K. and Ambraseys, N. (1990), ''Experimental behaviour of reinforced concrete walls under earthquake loading", *Earthq. Eng. Struct. Dyn.*, **19**(3), 389-407.

Fardis, M.N., Schetakis, A. and Strepelias, E. (2013), "RC buildings retrofitted by converting frame bays into RC walls", *Bull. Earthq. Eng.*, **11**(5), 1541-1561.

fib CEB-FIP (2010), *fib Model Code 2010 - Final draft, Volume 1*. Bulletin No. 65, International Federation for Structural Concrete, Lausanne, Switzerland.

Hannewald, P., Beyer, K. and Mihaylov, B. (2012), "Performance based assessment of existing bridges with wall type piers and structural deficiencies", *presented in the ACI341 Session: "Forming a Framework for Performance-based Seismic Design of Concrete Bridges", ACI Fall Convention*, Toronto, Canada.

Hiraishi, H. (1984), "Evaluation of shear and flexural deformations of flexural type shear walls", *Bull. NZ. Soc. Earthq. Eng.*, **17**(2), 135-44.

Jiang, H., Wang, B. and Lu, X. (2013), "Experimental study on damage behavior of reinforced concrete shear walls subjected to cyclic loads", *J. Earthq. Eng.*, **17**(7), 958-971.

Johnson, B. (2010), "Anchorage detailing effects on lateral deformation components of R/C shear walls", M.Sc. Thesis, University of Minnesota, Department of Civil Engineering, 353 pp.

Massone, L.M. and Wallace, J.W. (2004), "Load-deformation responses of slender reinforced concrete walls", *ACI Struct. J.*, **101**(1), 103-113.

Oesterle, R.G., Aristizabal-Ochoa, J.D., Fiorato, A.E., Russell, H.G. and Corley, W.G. (1979), "Earthquake resistant structural walls - tests of isolated walls: Phase II", Report to National Science Foundation. Skokie (IL, USA): PCA Construction Technology Laboratories.

Oesterle, R.G., Fiorato, A.E., Johal, L.S., Carpenter, J.E., Russell, H.G. and Corley, W.G. (1976), "Earthquake resistant structural walls - tests of isolated walls", Report to National Science Foundation. Skokie (IL, USA): PCA Construction Technology Laboratories.

Priestley, M., Seible, F. and Calvi, M. (1996), *Seismic Design and Retrofit of Bridges*, Wiley, New York, USA.

Syntzirma, D., Pantazopoulou, S. and Aschheim, M. (2010), "Load-history effects on deformation capacity of flexural members limited by bar buckling", *J. Struct. Eng.*, ASCE, **136**(1), 1-11.

Tastani, S.P. and Pantazopoulou, S.J. (2013a), "Yield penetration in seismically loaded anchorages: effects on member deformation capacity", *Earthq. Struct.*, **5**(5), 527-552.

Tastani, S.P. and Pantazopoulou, S.J. (2013b), "Reinforcement-concrete bond: state determination along the development length", *J. Struct. Eng.*, ASCE, **139**(9), 1567-1581.

Thomsen, J.H. and Wallace, J.W. (2004), "Displacement-based design of slender rc structural walls - experimental verification", *J. Struct. Eng.*, ASCE, **130**(4), 618-630.

Thomsen, J.H. and Wallace, J.W. (1995), "Displacement-based design of rc structural walls: an experimental investigation of walls with rectangular and T-shaped cross-sections", Report. No CU/CEE-95/06 to National Science Foundation, Dep. of Civil Engineering, Clarkson University.

Wallace, J.W., Massone, L.M., Bonelli, P., Dragovich, J., Lagos, R., Lüders, C. and Moehle, J. (2012), "Damage and implications for seismic design of RC structural wall buildings", *Earthq. Spectra*, **28**(1), 281-299.

Wallace, J.W. and Moehle, J. (2012) "Behavior and design of structural walls - Lessons from recent laboratory tests and earthquakes", *International Symposium on Engineering Lessons Learned from the 2011 Great East Japan Earthquake*, Tokyo, Japan.

CC